# We are IntechOpen, the world's leading publisher of Open Access books Built by scientists, for scientists

**4,800**
Open access books available

**122,000**
International authors and editors

**135M**
Downloads

Our authors are among the

**154**
Countries delivered to

**TOP 1%**
most cited scientists

**12.2%**
Contributors from top 500 universities

CLARIVATE ANALYTICS BOOK CITATION INDEX INDEXED

WEB OF SCIENCE™

Selection of our books indexed in the Book Citation Index in Web of Science™ Core Collection (BKCI)

## Interested in publishing with us?
## Contact book.department@intechopen.com

Numbers displayed above are based on latest data collected.
For more information visit www.intechopen.com

12

# Inelastic Collisions and Hypervelocity Impacts at Nanoscopic Level: A Molecular Dynamics Study

G. Gutiérrez, S. Davis, C. Loyola, J. Peralta, F. González,
Y. Navarrete and F. González-Wasaff
*Group of NanoMaterials*, Departamento de Física, Facultad de Ciencias,*
*Universidad de Chile*
*Chile*

## 1. Introduction

In this chapter we present an atomic level study of nano-particle impact using molecular dynamics simulation. Two cases have been considered. First, we simulate the bouncing of a ball over a surface due to a constant force (which mimic the gravity force), modeling the inter-atomic interaction by a modified Lennard-Jones potential, where the ball-surface atom interaction is represented by a purely repulsive term. The analysis of the results makes it possible, among other aspects, to determine the restitution coefficient in each bounce as well as to understand the processes of energy loss in inelastic collisions, which are actually not a loss, but a transfer to thermal and vibrational energy. The second simulation describes the impact mechanisms of a solid projectile hitting a target at high velocity. Both the projectile and the target are made of copper, which is modeled by a realistic many-body tight-binding potential. The projectile velocity is kept constant during all the simulation, representing an extreme condition, where the momentum and hardness of the projectile is much higher than the momentum and hardness of the target. In this regime, we identify two different behavior in dependence of the projectile velocity: at low velocities (less than 4 km/s) the target basically recover its structure after the passage of the projectile, but at higher velocities, the projectile left a permanent hole in the target.

Both problems, inelastic collisions and hypervelocity impacts, are non-equilibrium related phenomena which are important from a basic and applied point of view, in several areas of science: physics, materials science, aeronautics, mechanics, among others. From a theoretical point of view, they have been extensively treated in the macroscopic level, by using continuum hydrodynamic simulation, and only recently researchers are using molecular dynamic simulation, intended to an understanding of these phenomena at the scale of inter-atomic interactions. Besides the calculation of equilibrium properties and their associated fluctuations, molecular dynamics allows for a wider range of problems to be tackled: given that we have access to the atomic trajectories we can study the transit to equilibrium, as well as purely non-equilibrium phenomena (where we are interested not in the final state but in the process itself ), for instance, shock-induced plasticity and fracture of materials. In this regard, Non-Equilibrium Molecular Dynamics (NEMD) has emerged recently as a branch dealing with, and promising to shed light on, the mechanism behind these (and other similar) irreversible processes.

*www.gnm.cl

## 2. Molecular dynamics in non-equilibrium conditions

The framework to tackle the problems out of equilibrium is Non-equilibrium Statistical Mechanics. Its concerns the extension of the usual formalism of Statistical Mechanics (microcanonical, canonical and other extended ensembles, partition functions) to systems either approaching thermodynamic equilibrium after a perturbation, or definitely far away from it. So far there is no unified theory we can appropriately call non-equilibrium statistical mechanics [1], only a number of results applicable to processes in the linear response regime (thermodynamic fluxes proportional to the thermodynamic forces), such as the celebrated Onsager regression hypothesis (Callen, 1985) that relates the decay of macroscopic variables in a non-equilibrium setting to the regression of fluctuations in equilibrium. Prigogine's minimum entropy production (Prigogine, 1968) principle, also restricted to the linear response regime, is a possible explanation for the emergence of order in dissipative systems. The fluctuation-dissipation theorem and the Green-Kubo formulas (Zwanzig, 2001) determine transport coefficients from equilibrium measurements. There are also a few results valid arbitrarily far away from equilibrium, such as the family of fluctuation theorems (Evans & Searles, 2002) quantifying the likelihood of instantaneous violations of the Second Law of thermodynamics.

Non-equilibrium Molecular Dynamics (NEMD) is then the natural extension of molecular dynamics techniques to study non-equilibrium problems, and attempts to fill the void left by a missing theoretical framework.

Stationary (or *steady-state*) processes like deformation under shear stress, or a sample submitted under a temperature gradient, among others, require the implementation of NEMD under temperature control. In this case the use of thermostat algorithms is necessary to maintain the steady-state regime, extracting the excess heat generated by the process. However this has the drawback of modifying the equations of motion, introducing friction and noise forces which perturb the original dynamics (energy is not conserved), and affecting the performance of the usual numerical integration methods.

A comprehensive review of thermostat methods and their implementation in the context of NEMD is given by Hoover (Hoover & Hoover, 2007). Briefly, the standard implementation of the thermostat is the Nosé-Hoover equation of motion,

$$\frac{d\vec{p}_i}{dt} = \vec{F}_i - \zeta \vec{p}_i, \tag{1}$$

where $\zeta$ is a friction coefficient governed by

$$\frac{d\zeta}{dt} = \frac{1}{N\tau^2} \sum_{i=1}^{N} \left( p_i^2 / m k_B T_0 - 1 \right), \tag{2}$$

$T_0$ the imposed temperature and $\tau$ is a relaxation time, controlling the degree of coupling of the "thermal bath" with the system.

It is possible, however, to perform NEMD in a completely microcanonical way (i.e. without modifying Newton's equations) for systems outside the steady-state regime (for instance in

[1] The maximum caliber formalism (Jaynes, 1980; Stock et al., 2008), based on information-theoretic ideas, together with the maximum entropy production principle derived from it seem to show promising early results as such a unifying basis (Dewar, 2005; 2003; Kleidon et al., 2005).

the case of shockwave propagation (Holian, 1995), collisions, fast fracture, detonations) where it is not necessary to remove the excess heat. Here energy is conserved, being converted from kinetic or elastic into thermal, vibrational and other forms, the heat eventually produced in the process remains inside the system, causing an increase in temperature and eventually being able to induce local melting. This kind of NEMD simulations are justified because we are implicitly solving the Liouville equation,

$$\frac{\partial P(\mathbf{p},\mathbf{q})}{\partial t} = -\{P,\mathcal{H}\}, \tag{3}$$

which describes the evolution of the phase space distribution function $P(\mathbf{p},\mathbf{q})$ of a system of particles obeying Newton's equations, and this is valid arbitrarily away from equilibrium.

It is important to consider that, away from the linear response regime, there is no unique definition of thermodynamic intensive variables such as temperature, pressure or chemical potential if those variables are not fixed (Casas-Vásquez & Jou, 2003). However, the usual practice is to take the instantaneous kinetic energy of the system (or even of a region of the system) to evaluate an instantaneous "kinetic" temperature,

$$T_K(t) = \frac{m}{3k_B}\sum_{i=1}^{N} v_i^2. \tag{4}$$

When using the instantaneous kinetic energy to evaluate a local instantaneous temperature, it might be required to remove the translational part of the velocities for the atoms in the region, if they happen to have non-zero linear momentum. For instance, a projectile approaching a target cannot be assigned a higher temperature by virtue of its translational speed.

It is also possible to evaluate an instantaneous "configurational" temperature (Baranyai, 2000),

$$T_C(t) = \frac{1}{k_B}\frac{|\nabla\Phi(t)|^2}{\nabla^2\Phi(t)}, \tag{5}$$

where $\Phi$ is the potential energy function, which depends on $t$ only through the atomic positions. Away from equilibrium both definitions (kinetic and configurational) do not necessarily coincide, because an object immersed in the non-equilibrium system and used as a thermometer could equilibrate in different time scales to the configurational and kinetic degrees of freedom and therefore measure different temperatures. In fact "operational" definitions of non-temperature exist that measure the kinetic energy of a tracer (probably heavier) particle placed inside the system, and assumed to be in thermal equilibrium with it.

In the following, we briefly describe the molecular dynamic method and its implementation our in-house code *Las Palmeras Molecular Dynamics*. Next, the inelastic collisions and hypervelocity impacts simulations are presented, as examples of the potential of an atomic-level description. Finally, general conclusions are drawn.

## 3. Las Palmeras Molecular Dynamics

Although there are many general purpose MD codes, they are usually subjected to design limitations arising mostly due to efficiency considerations. A given code is usually optimized to perform extremely well for one kind of system (for instance bulk systems) but because of

said optimization it performs poorly on a different kind of system. This, in practice, only allows the study of certain systems and conditions.

Most codes cannot handle in an easy way the requirements of some setups, such as non-periodic boundary conditions, non-negligible variations of density inside a sample, or initial states prepared far from equilibrium. It might be possible to modify these codes to lift some of the limitations, but it could be cumbersome and error-prone. For these cases, a more flexible MD code is needed, even though some performance could be sacrificed.

We could say that the early way of doing MD was to implement a tailor-made computer program with precisely the chosen algorithms for numerical integration of the equations of motion and computation of the interatomic potentials and forces. Thus, one different computer code for each system to be simulated.

The next stage in MD computer codes is the ability to choose the interatomic potential at runtime (i.e., every time the program is executed, without the need to recompile for every change) along with all the other options such as the time step used for integration, total simulation time, initial conditions of pressure and temperature and so on. This has led to general purpose MD codes such as Moldy (Refson, 2000) and DL_POLY (Smith & Forester, 1996) among many others. While the ability to choose the potential function is commonplace nowadays, very few computer codes offer the choice of changing the integration algorithm at runtime, although several have the choice at compile-time (i.e., during the compilation stage).

From a general point of view, the MD procedure consist of four main stages, namely: (a) the initialization of the sample, (b) the calculation of interatomic forces, (c) the integration of the equations of motion, and (d), collecting statistics and the computation of properties. It work quite well in several different cases, like equilibrium conditions or even for metastable system, like glasses (see, for example (Gutiérrez et al., 2010)). But also MD procedure can be applied to more extreme conditions.

When the MD simulation that we intend to perform is not standard, for example in the case of simulations far away from thermodynamic equilibrium (shockwaves (Loyola et al., 2010), high velocity impacts, ) or non-standard potential functions and forces (for example friction forces or external fields) one can clearly see the need for an hybrid approach between the tailor-made MD code (containing exactly the algorithms we need for a given simulation) and the general purpose MD code (with several choices available at run-time and compile-time). We would want to replace pieces of the program at will, including (but not limited to) integration methods, potential functions and other algorithms, such as the one responsible for computing interatomic distances or the thermostat algorithms used to control the applied temperature or pressure in an isothermal-isobaric (NPT) MD simulation. Here the general purpose approach is not general enough, only allowing some limited choices.

Our motivation for writing yet another MD code, *Las Palmeras Molecular Dynamics* (LPMD) (Davis et al., 2010) is to fill this practical void. LPMD is designed as a completely modular MD code, consisting of a set of interchangeable pieces or *plug-ins* which can be linked together in different ways to accommodate the needs of a non-standard MD simulation. Beyond that, the user can also perform post-simulation analysis, convert between input/output formats, prepare samples with ease and visualize simulations in real time. LPMD's modular design also improves efficiency in some cases. It also allows the user to add new pieces (integration methods, interatomic potentials, properties, file formats, and many others) without the need for learning the complete code architecture. LPMD is open source software written in standard C++ language, and released under the General Public License

(GPL) version 3. Figure 1 displays an example of the control file. For more information, visit `www.lpmd.cl`.

```
#This is a comment. Comments are used usually as a title:
########################################
# System file of Au crystal using LPMD  #
########################################
cell cubic 28.56
input module=lpmd file=300K-Gold.lpmd level=1
output module=lpmd file=au.lpmd each=15 level=1
periodic false true true
steps 5000

#Integrator
use velocityverlet as vv
    dt 1.0
enduse

#CellManager

use linkedcell
     mode auto
     cutoff 7.5
enduse

# Sutton-Chen Potential (parameters for gold)
use suttonchen as sc
    e 0.013
    n 10
    a 4.08
    m 8
    c 34.408
    cutoff 7.5
enduse

#- Applying Plugins -#
integrator vv
cellmanager linkedcell
potential sc Au Au
```

Fig. 1. Example of an LPMD control file. The components are loaded (`use...enduse`) and then applied.

### 3.1 Structural properties with LPMD

We will denote by structural property, any quantity $A_S$ which depends on the instant $t$ only through the atomic coordinates,

$$A_S(t) = A_S(\vec{r}_1(t), \ldots, \vec{r}_N(t)), \tag{6}$$

with $N$ the number of particles.

LPMD allows the calculation of several structural properties (either as instantaneous values or as averages), including the radial distribution function $g(r)$ (using the `gdr` plug-in) and common neighbor analysis (through the `cna` plug-in), both of which can be used to measure a degree of deviation from an ideal crystal structure.

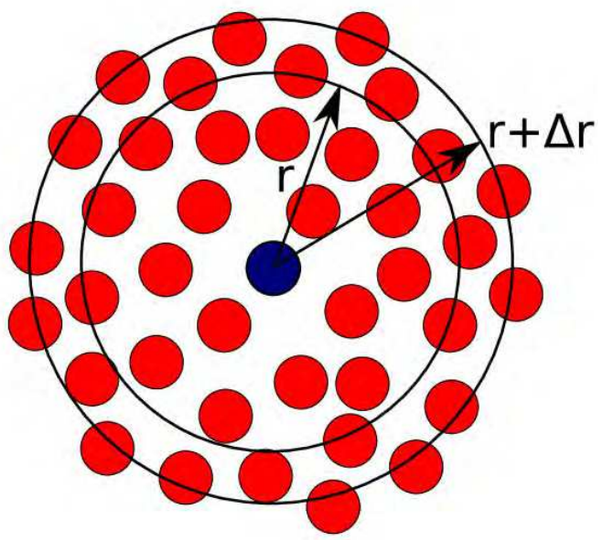


Fig. 2. Schematic representation of the computation of the radial distribution function $g(r)$.

The radial distribution function $g(r)$ represents the probability density for finding a neighboring atom at a distance $r$, normalized to the same probability density in a perfectly uniform distribution of atoms. This ensures that $g(r)$ goes to unity for large enough $r$, independently of the system. It is formally defined as

$$g(r) = \frac{V}{N^2} \left\langle \sum_i \sum_{j \neq i} \delta(\vec{r} - \vec{r_{ij}}) \right\rangle . \tag{7}$$

where $N$ is the total number of atoms in the system and $V$ is the total volume. However, in practice, it is computed from an histogram of the neighbor distribution,

$$g(r) = \frac{V}{N} \frac{n(r)}{\frac{4}{3}\pi((r+\Delta r)^3 - r^3)} \approx \frac{V}{N} \frac{n(r)}{4\pi r^2 \Delta r} \tag{8}$$

where $n(r)$ is the number of atoms in the spherical shell between $r$ and $r + \Delta r$ (see figure 2).

The Common Neighbor Analysis (CNA) (Honeycutt & Andersen, 1987) is a technique used in atomistic simulations to determine the local ordering in a given structure. CNA gives more detailed information than the radial distribution function $g(r)$, as it considers not only the number of neighbors at a given distance but also their location with respect to other common neighboring atoms. In the CNA method (see figure 3), every pair of atoms is labeled according to four indices $(i, j, k, l)$: the first index, $i$, is 1 for nearest neighbor pairs, 2 for next-nearest neighbors, and so on. The second index, $j$, corresponds to the number of *common neighbors* shared by the atoms in the pair. The third index, $k$, corresponds to the number of *bonds* that can be "drawn" between the $j$ common neighbors (taking the bond length as the nearest neighbor distance). Finally, the fourth index, $l$, corresponds to the length of the longest chain that connects all the $k$ bonds. The different structures have the following distribution of pairs: FCC has only **1-4-2-1** pairs, in hcp the pairs are distributed equally between **1-4-2-1** and **1-4-2-2**, and in bcc there are **1-4-4-4** and **1-6-6-6** present in ratios $3/7$ and $4/7$, respectively.

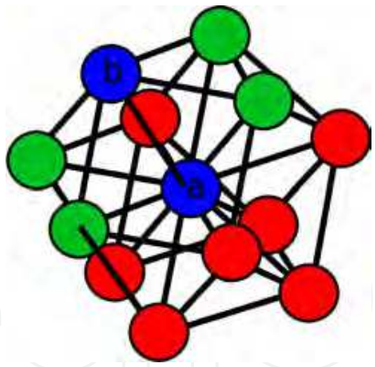


Fig. 3. Four common neighbors (green atoms) of the pair *a-b* (in blue) in a face-centered cubic structure. The pair depicted as *a-b* has indices 1-4-2-1 in CNA notation, and is the only kind of pair appearing in the FCC structure.

## 4. Bouncing of a ball over a surface: atomic level study

A typical problem in classical mechanics is the bouncing of a bead in free fall over a surface, due to the action of the force of gravity (Alonso & Finn, 1992; Eisberg & Lerner, 1981). After each bouncing, the body reaches different heights, each one of them less or equal than the previous one. The most common explanation for this phenomenon is the viscoelastic dissipation, which results in an energy loss due to the inelastic collision (Aguirregabiria et al., 2008; Falcon et al., 1998).

Although there have been many works dealing with the dynamics of inelastic collisions (Goldsmith, 2001; Johnson, 1987; Zukas et al., 1982) and many measurements of the energy loss in such collisions (Bridges et al., 1984; Goldsmith, 2001; Hatzes et al., 1988; Lifshitz & Kolsky, 1964; Lun & Savage, 1986; Raman., 1918; Reed, 1985; Supulver et al., 1995; Tabor, 1948; Tillett, 1954; Tsai & Kolsky, 1967; Zener, 1941), there is a considerable scatter in existing data, and the mechanisms of dissipation and the behavior of the restitution coefficient with the impact velocity are still open problems (Falcon et al., 1998). At high impact velocities, i.e., when fully plastic deformations occur, this behavior is well known both experimentally (Goldsmith, 2001; Raman., 1918; Reed, 1985; Tabor, 1948; Tillett, 1954; Zener, 1941) and theoretically (Goldsmith, 2001; Johnson, 1987; Tabor, 1948), but the mechanisms of energy loss during a collision are hard to track at a macroscopic level.

Molecular dynamics allows us to keep track of the position and velocity of every particle in the system at any instant of time. Using statistical mechanics, the calculation of energy, temperature and other thermodynamic properties is straightforward. Moreover, if the target (surface) is considered as being a part of the system, the total energy remains constant, and the "energy loss" that the bead experiments is just a transfer of translational kinetic energy to internal potential and thermal energy, which can be identified with mechanisms of energy loss, such as plastic deformation, vibrational energy and others.

To show how this phenomenon occurs, molecular dynamics simulations were performed using the LPMD program(Davis et al., 2010) (see section 3). A bead is dropped from rest at different heights in a constant force field over a surface. The resulting collisions show two main types of deformation: slight deformation, where the bead remains vibrating after the collision, and substantial deformation, where the bead changes its shape. Then, the evolution of the different energies in time is computed in order to show in detail the energy transfer.

### 4.1 Simulation details

The system consist of a solid ball that interacts repulsively with a solid surface, both made of argon in the solid state (see figure 4). The interaction between atoms separated by a distance

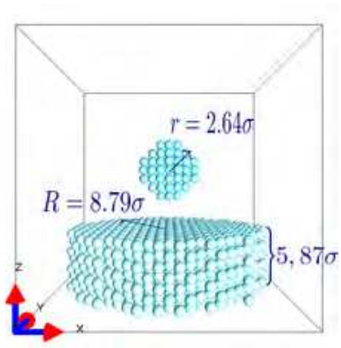


Fig. 4. Argon ball over a solid argon surface, immersed in a constant force field. Image generated by the LPVisual plugin of the LPMD program.

$r$ is modeled using a modified form of the Lennard-Jones potential (Barrat & Bocquet, 1999):

$$V(r) = \begin{cases} 4\varepsilon \left[ \left(\frac{\sigma}{r}\right)^{12} - c \left(\frac{\sigma}{r}\right)^{6} \right] & r < r_c = 2.5\sigma \\ 0 & r \geqslant r_c \ , \end{cases} \tag{9}$$

where $r_c$ is a cut-off chosen here to be $2.5\sigma$ ($\sigma$ is the Lennard-Jones diameter and $\varepsilon$ is the depth of the potential well). For our system, the parameters $\varepsilon/k_B = 119.8$ K and $\sigma = 3.40$ Å are the same for all atoms and correspond to the values for argon (Kittel, 2005), whose atomic mass is $M = 39.948$ amu. In the rest of this section, all quantities are expressed in LJ reduced units, using $\sigma$, $\varepsilon$ and $M$ as length, energy and mass scales, respectively [2].

The interaction between atoms in the ball and atoms in the surface is given by the equation (9) with $c = 0$ (i.e., purely repulsive), while the interactions between any pair of atoms in the ball is given by the usual Lennard-Jones potential (eq. (9) with $c = 1$). The last also holds for every pair of atoms inside the surface. The Newton equations of motion are integrated using the Beeman algorithm, with a time step $\Delta t = 4.651 \times 10^{-4} \tau$.

The solid ball and the surface slab were equilibrated at zero temperature for $5 \times 10^3$ time steps to allow them to adopt relaxed configurations.

The ball, composed of less than 100 atoms, was immersed in a constant force field in the direction of the negative $z-$axis, whose magnitude was $0.026\, F_0$, and it was dropped from different heights over the surface, composed of about 1500 atoms. This force produces a constant acceleration of the center of mass of the ball of $0.026\, a_0$, which means that it travels $0.49\, \sigma$ after a time $\tau$ of being dropped. Each simulation took about $3 \times 10^4$ time steps ($\sim 14\, \tau$).

Different types of collisions were observed. The most representatives are shown in figures 5 and 6. Figure 5 shows one of the simulations where the ball is falling over the surface. In

[2] Time: $\tau \equiv \sigma\sqrt{M/\varepsilon} = 2.15$ ps.
Velocity: $v_0 \equiv \sqrt{\varepsilon/M} = 157.91$ m/s.
Acceleration: $a_0 = \varepsilon/M\sigma = 0.73$ Å/ps$^2$.
Force: $F_0 \equiv \varepsilon/\sigma = 3.04 \times 10^{-3}$ eV/Å.

this case, the ball was dropped from $z = 11.03\,\sigma$. While the ball is hitting the surface, it gets compressed, and then leaves the ground, oscillating harmonically (figures 5(c) and 5(d)).

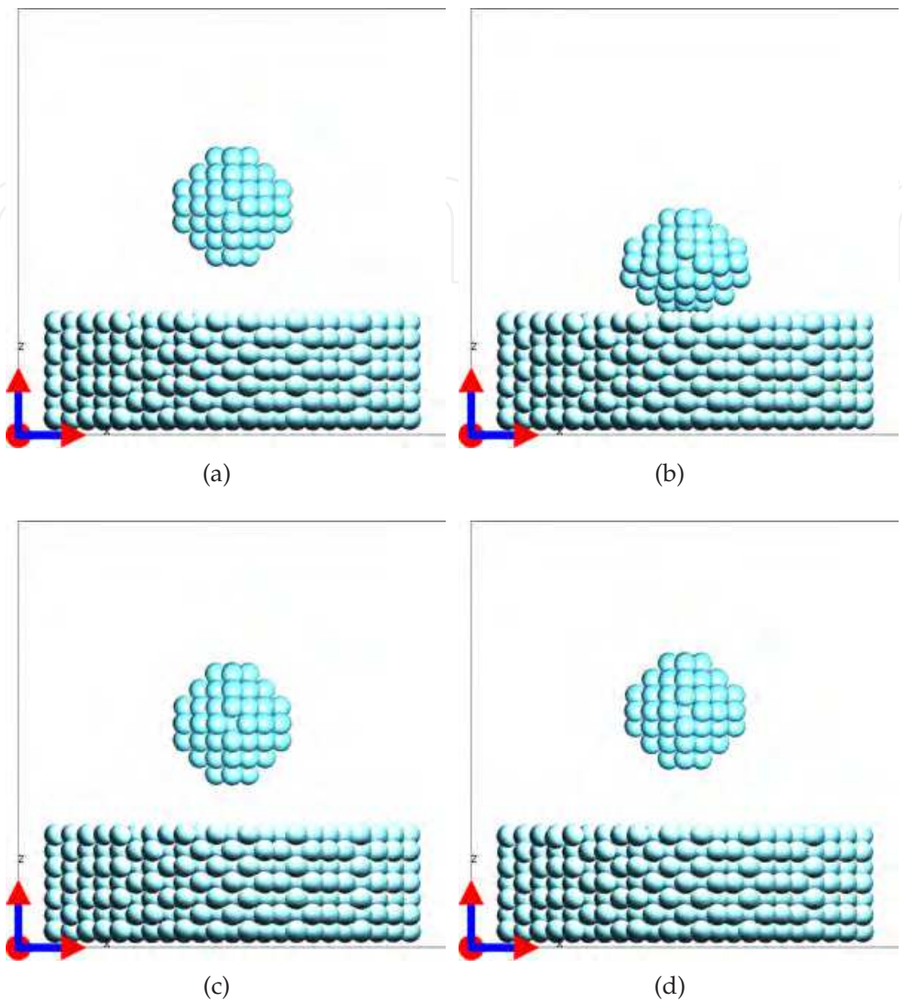


Fig. 5. Ball dropped from $z = 11.03\,\sigma$. (a) The ball is falling towards the surface. (b) The ball hits the surface and gets compressed, inducing an oscillatory movement on it. (c) The ball leaves the surface vibrating. A maximum amplitude is reached. (d) A minimum amplitude is reached due to the induced oscillatory movement. The maximum amplitude is slightly greater than the minimum, so the difference between the size of the ball in 5(c) and its size in 5(d) is not clearly appreciated. You can see the simulations at `www.lpmd.cl` in the examples section, where these oscillations can be clearly appreciated in the videos.

Figure 6 shows another simulation, where the ball was dropped from $z = 28.15\,\sigma$. After the collision, the ball acquires a new shape.

### 4.2 Results

In this section we present the results of several simulated collisions. The ball was dropped from heights $h_0$ between $11.03\,\sigma$ and $79.53\,\sigma$. We begin by describing the dynamics of the ball and discuss about the height reached after each bounce. Then, we analyze the deformation

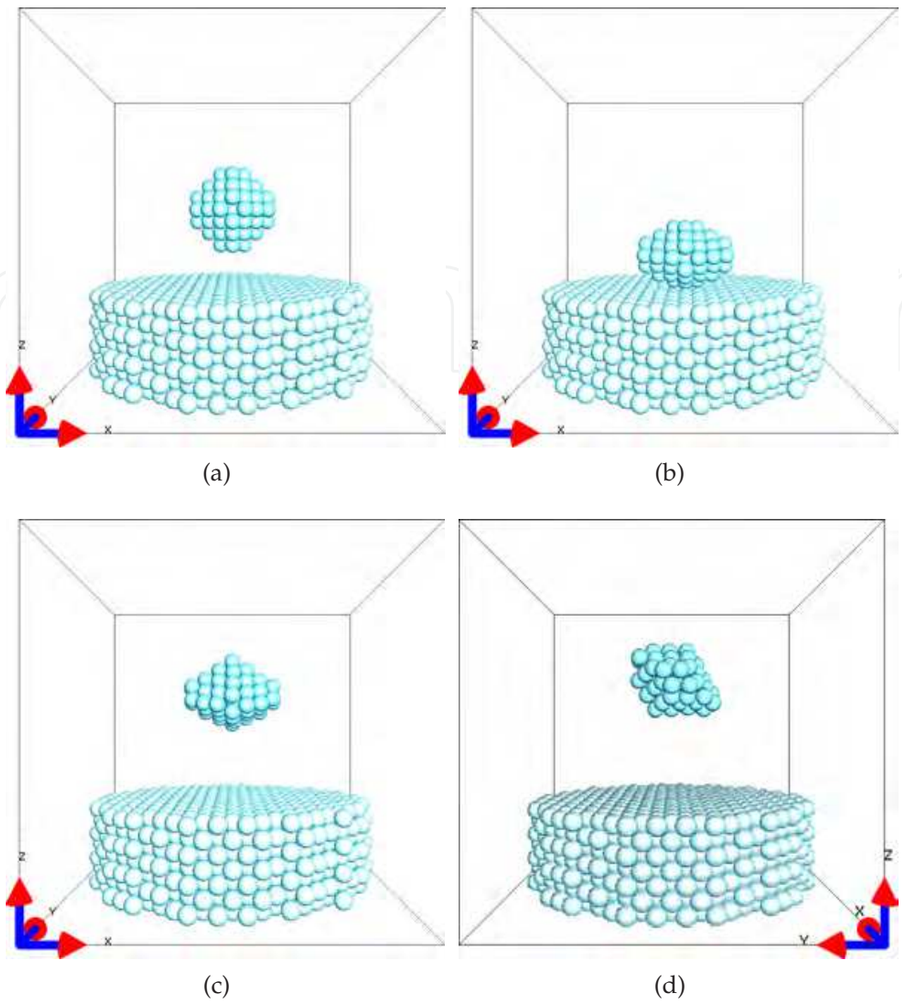


Fig. 6. Ball dropped from $z = 28.15\,\sigma$. (a) The ball is falling towards the surface. (b) The ball hits the surface and gets compressed. (c) The ball lifts the surface acquiring a new shape, with almost none internal vibrations. (d) The ball keeps its new shape after the collision.

of the ball by evaluating the pair-distribution function $g(r)$. Finally, we classify kinetic and potential energies in different types and then examine how these energies are transferred from one to another to keep the total energy constant.

#### 4.2.1 Heights reached

Fig. 7 shows the heights reached by the center of mass of the ball after each bounce. The zeroth bounce represents the initial height $h_0$. The case in which the ball is dropped from a height of $11.03\,\sigma$ corresponds to a quasi-elastic bounce because the height of bounces are almost the same. When $h_0 = 18.64\,\sigma$, the height reached by the ball after the first bounce is smaller than the initial height from where it was dropped, and something similar happens with the other bounces: the maximum heights reached decrease until the ball remains static over the target. For $h_0 = 41.47\,\sigma$, the maximum height reached after the first bounce is considerably smaller than $h_0$. Big differences of height are observed also for $h_0 = 58.6\,\sigma$, where a notorious

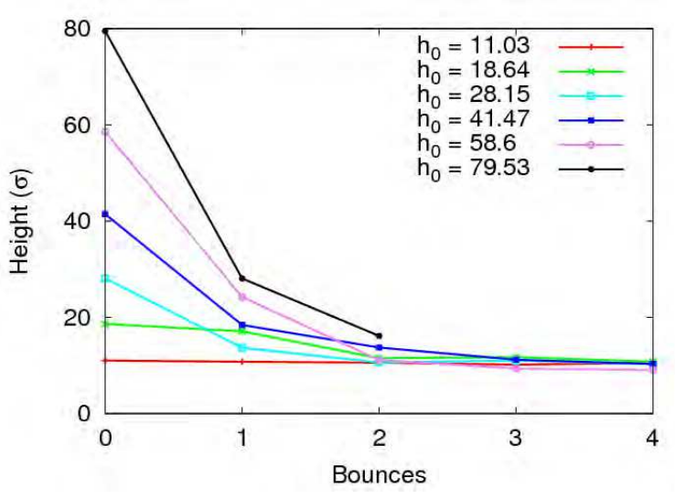


Fig. 7. (Color online) Maximum heights reached after each bounce, by the center of mass of the ball.

decrease is appreciated in the first bounce as well as in the second. For $h_0 = 79.53\,\sigma$ only two bounces are observed because, after the first bounce, the ball gets deformed and loses its solid structure, which does not allow it to keep bouncing. Nevertheless, a common behavior is observed for all cases: after the third bounce, the height reached is almost the same. At this point, the ball remains over the surface.

#### 4.2.2 Deformation of the ball

We analyze in detail the structure of the ball evaluating the pair-distribution function $g(r)$ for the atoms that constitute the ball for different time steps (Fig. 8) in different simulations.

Before the first impact, i.e., when the ball is falling, it has a FCC structure (for any $h_0$), because the first neighbors are clearly appreciated at $1.09\,\sigma$ for all cases (Fig. 8), which is the known value for first neighbors in argon lattice structure (Kittel, 2005). In Fig. 8(a) it can be seen that for times between $t = 0$ and $t = 5.581\tau$ the initial FCC structure is conserved, despite of the effects of the impacts with the surface, which took place at $t = 0.71\,\tau$, $t = 2.07\,\tau$, $t = 3.38\,\tau$, $t = 4.52\,\tau$ and $t = 5.83\,\tau$. The peaks also have similar widths, which means that there are small temperature effects. If $h_0$ is increased, the peaks become wider and smaller (Fig. 8(b) to 8(c)) but still distinguishables, which implies a rising of the temperature inside the ball without melting. We will analyze this subject deeper in the next section (4.2.3). In the latter case (Fig. 8(c)), the ball acquires a new solid structure (Fig. 6), that seems to be, just looking at the $g(r)$ function, still FCC type. For $h_0 > 41.47\,\sigma$ (Fig. 8(d) to 8(f)) just one peak is distinguishable as long as the distance $r$ to an atom increases, which means that an atom has, in average, a neighbor at $1.09\,\sigma$ and no well defined second neighbors or further. This can be interpreted as the melting of the ball.

#### 4.2.3 Energy

In an inelastic collision, the dissipation of energy of a body is given by the energy transfer from mechanical energy to internal energies, such as thermal energies and vibrational energies, being the last one the responsible of plastic deformations of the body. Since our simulations consider the surface as part of the system, no dissipation is observed, because the total energy

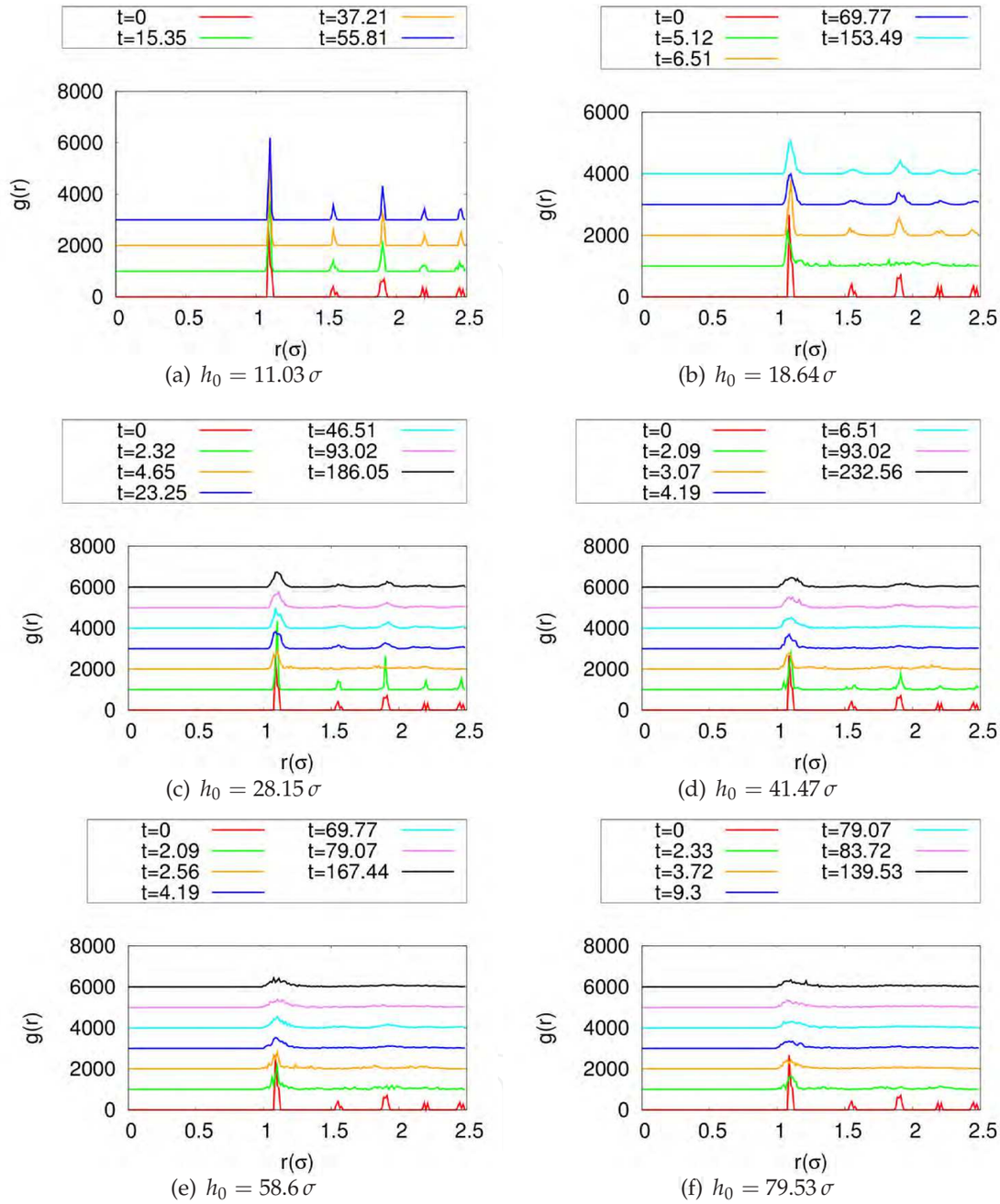


Fig. 8. (Color online) Pair-distribution functions calculated for the atoms in the ball, for different times (see inset in $\tau/10$). Each graph corresponds to different initial heights $h_0$. The pair distribution function for each $t$ at $h_0$, has been shifted upwards for clarity.

remains constant. The internal energies of the ball change in each bounce, and the mechanism of loss and gain of energy are explained by considering the following classification of energies:

The velocity of the center of mass of the ball ${\mathbf{V}_{\mathrm{CM}}}^B$ is calculated for each time-step to compute the **translational kinetic energy of the ball**, defined by

$$K_B = \frac{1}{2} M_B \| {\mathbf{V}_{\mathrm{CM}}}^B \|^2, \tag{10}$$

where $M_B = 79\,M$ is the mass of the ball. The velocity of the center of mass of the surface ${\mathbf{V}_{\mathrm{CM}}}^S$ is calculated for each time-step to compute the **translational kinetic energy of the surface**, defined by

$$K_S = \frac{1}{2} M_S \| {\mathbf{V}_{\mathrm{CM}}}^S \|^2, \tag{11}$$

where $M_S = 1444\,M$ is the mass of the surface. For a given time step, the difference between the velocity of the center of mass ${\mathbf{V}_{\mathrm{CM}}}^B$ and the velocity of the atom $i$, $\mathbf{v}_i$, defines $\bar{\mathbf{v}}_i = \mathbf{v}_i - {\mathbf{V}_{\mathrm{CM}}}^B$, the velocity of the atom $i$ relative to the center of mass of the ball, which is used to define the kinetic energy of the ball relative to its center of mass, what we call **thermal energy of the ball**, by

$$T_B = \sum_{\substack{\text{all ball} \\ \text{atoms}}} \frac{1}{2} m_i \| \bar{\mathbf{v}}_i \|^2, \tag{12}$$

where $m_i = M$ is the mass of the atom $i$. In the same way, we define the **thermal energy of the surface** by

$$T_S = \sum_{\substack{\text{all surface} \\ \text{atoms}}} \frac{1}{2} m_i \| \bar{\mathbf{v}}_i \|^2, \tag{13}$$

where, in this case, $\bar{\mathbf{v}}_i = \mathbf{v}_i - {\mathbf{V}_{\mathrm{CM}}}^S$. Now, since the interaction between any pair of atoms is given by equation (9), the total potential energy $U$ is given by the sum over all pairs of atoms plus the energy given by the force field, $U_F = M_B\, a\, z_{\mathrm{CM}}$, where $a = 0.026\,a_0$ and $z_{\mathrm{CM}}$ is the $z-$axis coordinate of the center of mass of the ball. We divide the sum in four terms as follows:

$$U = V_B + V_S + U_c + U_F. \tag{14}$$

The first term corresponds to the potential energy of the ball, which keeps together all the pairs that belong to the ball, and we can associate it to a **vibrational energy of the ball**:

$$V_B = \sum_{\substack{\text{all ball} \\ \text{atoms}}} V(r). \tag{15}$$

The second term corresponds to the potential energy of the surface, which keeps together all the pairs that belong to the surface, and we can associate it to a **vibrational energy of the surface**:

$$V_S = \sum_{\substack{\text{all surface} \\ \text{atoms}}} V(r). \tag{16}$$

The third term corresponds to the potential energy generated by the interaction of an atom of the ball with an atom of the surface, i.e., between atoms of different types. We will refer to this term as collisional energy:

$$U_c = \sum_{\substack{\text{all} \\ \text{ball-surface} \\ \text{atom pairs}}} V(r). \tag{17}$$

The last term $U_F$ was already explained and corresponds to the potential that generates the force field.

Fig. 9 shows the evolution of all these energies in time, except for $V_S$, which is a negative term that remains almost constant and does not add additional information to the phenomenon. The energies are expressed in the Lennard-Jones energy unit, $\varepsilon$. The energy $U_F$ has been shifted $2\,\varepsilon$ downwards and $V_B$, $400\,\varepsilon$ upwards to keep all energies in the same range, since what matters is the changes in energy rather than their absolute values. Other cases, where the ball was dropped at different $h_0$, are quite similar in shape, but some peaks are bigger than others.

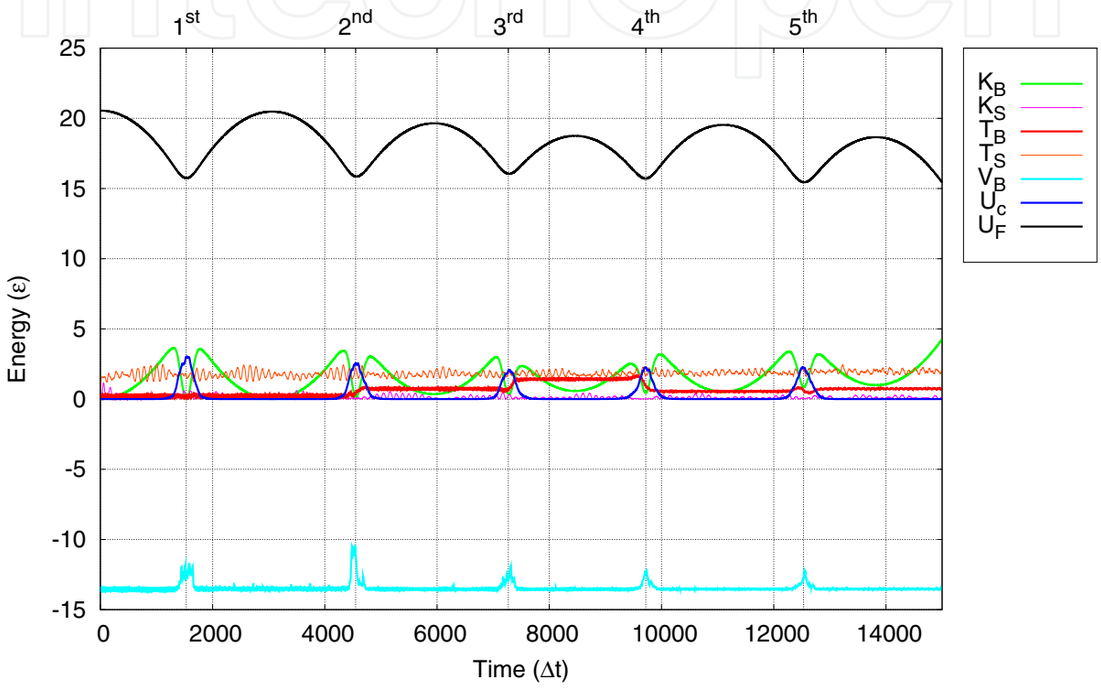


Fig. 9. (Color online) Evolution of the different energies in time for the simulation where the ball was dropped from $h_0 = 11.03\,\sigma$.

In the Fig. 9 it can be observed that the translational energy of the ball has several local minima, located between two maxima placed symmetrically around each of them. These minima represent the instant in which the kinetic translational energy $K_B$ vanishes, i.e., when the ball is completely stopped over the surface during a bounce. The maximum at the left hand of each minimum shows the instant in which the velocity of the center of mass of the ball acquires its maximum value before it begins to stop. The repulsive potential of the surface is equivalent to a force exerted upwards, but this force does not reduce velocity of the ball immediately, in fact, the velocity keeps growing with time before reaching the maximum, but its rate of change, that is, its acceleration, is reduced. Considering just the $z$ coordinate of the velocity of the center of mass, the first derivative of $K_B$ is given by

$$\frac{dK_B}{dt} = M_B V_{\mathrm{CM}}^B \dot{V}_{\mathrm{CM}}^B = M_B V_{\mathrm{CM}}^B A_{\mathrm{CM}}^B,$$

where $A_{\mathrm{CM}}^B$ is the acceleration of the center of mass of the ball. This derivative vanishes whether the velocity or the acceleration is zero, this is, when the net force exerted over the

ball is zero. This happens at the minima and maxima of $K_B$, so the maxima show where the force exerted by the surface equals the force $F = M_B\, a = \|\nabla U_F\|$.

When the ball has reached the point of maximum velocity, that is, the impact velocity, the velocity begins to decrease, because now the acceleration (and so the net force) is directed upwards. The ball reaches the point of null velocity (the minima) and then keeps accelerating until a maximum velocity that, for the first bounce, is the same as the impact velocity. In this interval of time, the energy $U_c$ becomes greater while the energy $K_B$ and $T_S$ decreases, which means that most of the energy was stored in the collision energy and a little bit in the vibrational energy of the surface, with almost no energy transferred to the thermal energy of the ball ($T_B$). In the second bounce (see labels above Fig. 9), much of the energy is transferred to the collision energy $U_c$, but now a little bit of energy is now transferred to the thermal energy of the ball $T_B$, so the ball lose translational energy and the maximum velocity after the collision (the departure velocity) is smaller than the impact velocity, so it is not able to reach the same height than before the collision. In the third bounce, the thermal energy of the ball is transferred back to kinetic translational energy, and the ball can reach a departure velocity greater than the impact velocity. Something similar happens with the fourth bounce, and what all bounces has in common is that the fluctuations of the thermal energy of the ball $T_B$ are comparable to the fluctuations of its vibrational energy $V_B$ and the thermal energy of the surface $T_S$.

Finally, we want to mention that, since $U_c$ is non-zero only when atoms of the ball are close to atoms of the surface, this energy gives a reasonable definition of the collision time as the width of the peak generated by this energy in each bounce.

In conclusion, a molecular dynamics study of the behavior of a ball bouncing repeatedly off a surface, considered as part of the system, has been done. We have observed that a study of the different types of energies of the system clearly shows what may be considered as the duration of a collision which, in contrast with typical macroscopic classical mechanics considerations, is not instantaneous, but a non negligible time interval. We have also shown that, despite of the fact that the collision is actually a continuous process that does not allow us to determine the "instant just before the collision" and the "instant just after the collision", which are always mentioned in macroscopic problems of momentum conservation, the impact velocity (maximum velocity reached before the ball stops) and the departure velocity (maximum velocity reached after the ball stops) can be determined precisely. This makes possible to determine the restitution coefficient in each bounce, a well studied property of bouncing systems, as the usual quotient of these velocities. The study of these energies have also helped to understand the processes of energy loss in inelastic collisions, which are actually not a loss, but a transfer to thermal and vibrational energy, within others. We could conclude that the force exerted by the surface acts as a break for the ball, and this force is the responsible for the decrease of the acceleration of the ball to zero (where the net force is null). So the impact velocity (maximum velocity reached before hitting the surface) is reached after the ball begins its collision with the floor, which can be considered as the moment in which the energy $U_c$ becomes relevant. It is clear that $K_T + U_F$ is constant when the collision is not taking place, but when it happens, in all bounces, despite of the fact that the collision energy $U_c$ behaved similar in every bounce, it was the most important among the energies in the collision, since it stores most of the "dissipated" energy by the ball, more than the vibrational energy transferred to the surface. The other energies, in spite of their changes, do not contribute significantly to the energy transfer.

## 5. Hypervelocity impact of projectiles

Hypervelocity impact of projectiles is of great interest in basic and applied research, and it is present in areas such as engineering and physics of materials, including civilian and military applications, among others. For example, since the development in the 1980's of cluster beam technology, the quality of the beams and the number of applications continues to grow (Jacquet & Beyec, 2002; Kirkpatrick, 2003; Popok & Campbell, 2006), as is the case of the materials which are bombarded with cluster beams in order to clean or smooth their surface or to analyze their composition, as well as to consolidate clusters. In several cases the effect of the cluster beams result from the combined effects of a single impact, which occurs separately and independently (Hsieh et al., 1992). Therefore it is important to understand the dynamics of such a single impact. In the field of space applications, hypervelocity impacts are being studied to see the damage they produce on ceramic tiles when nano and micrometeorites hit satellites, spacecraft and space stations. Because the experimental study at such high velocities (ranging from 3 km/s to 15 km/s approximately) is extremely difficult, computer simulation is an ideal tool to deal with them.

In the following we will study, by classical molecular dynamics simulations, the impact of a cluster composed of 47 atoms of copper (Cu) on a solid target of approximately 50 000 atoms of copper. The main goal is to depict the structural response of the target with respect to three different velocities of impact, 1.5 km/s, 3.0 km/s and 5.0 km/s. There will be a detailed description of the different processes, emphasizing the structural changes suffered by the target.

### 5.1 Computational procedure

The impact simulations were performed at high speeds with classical molecular dynamics, using the computer program *LPMD* (Davis et al., 2010). To simulate the impact of a projectile on a target, we initially built a cubic box of edge 86.64 Å containing 55,296 copper atoms in a FCC structure, which is used as target. This target was thermalized to 300 K through rescaling of velocities, for 15,000 time steps with $1\Delta t = 1$ fs. Then it was allowed to evolve without temperature control for another 15,000 time steps. The projectile is spherical in shape with a diameter of approximately 8 Å (one tenth the length of the edge of the target). Both projectile and target were placed in a tetragonal simulation cell length $x = y = 198.55$ Å and $z = 249.09$ Å, centered at $x$ and $y$, and separated by a distance 11 Å in $z$, as is shown in Figure 10.

The atomic interaction is represented by the empirical many-body Sutton-Chen potential,

$$\phi = \varepsilon \left\{ \sum_{i=1} \sum_{j=i+1} \left( \frac{a}{r_{ij}} \right)^n - c \sum_{i=1} \left[ \sum_{j=1, j \neq i} \left( \frac{a}{r_{ij}} \right)^m \right]^{1/2} \right\}, \tag{18}$$

where $\varepsilon = 0.0124$ eV, $a = 3.61$ Å (Cu lattice parameter), and $c = 39.432$, $n = 9$, $m = 6$ are adimensional parameters.

The simulations we perform used three different velocities for the projectile: 1.5 km/s, 3.0 km/s and 5.0 km/s, while the target is at rest. The projectile velocity is kept constant during all the simulation, irrespective of the friction or the force exerted by the target. Although this is not a real situation, it represent an extreme condition, where the momentum and hardness of the projectile is much higher than the momentum and hardness of the target.

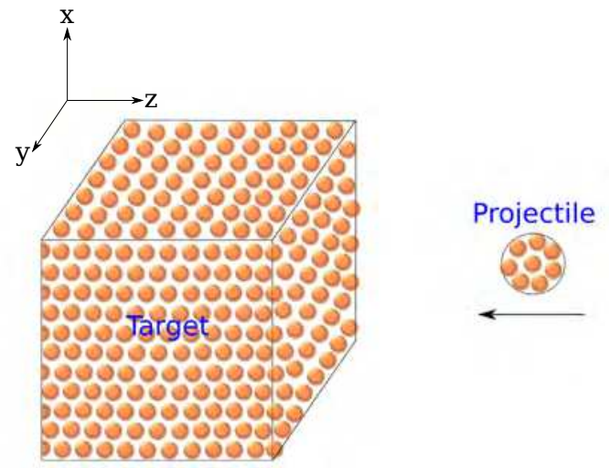


Fig. 10. Cu spherical projectile with velocity $-v_z$. Both are sitting in the $xy$ plane of the simulation box

In the following we present a detailed description of the different processes, emphasizing the structural changes suffered by the target. To perform the analysis of the target in a better way, atoms belonging to the projectile were removed and the target was divided into two radial sections.

### 5.2 Results

In Figure 11 is shown a general view of the passage of the projectile, in this case corresponding to 1.5 km/s. As can be seen, it melts the sample locally when it is going through. After the passage of the projectile, there are two regimes on the behavior of the target: 1) to certain speeds, including 1.5 and 3.0 km/s, the sample returns to its initial fcc structure, but with at higher temperature and with dislocations of planes, and 2) for speeds equal to or greater than 5.0 km/s, the projectile left a hole in the target and even though the atoms regroup in the same way, the target as a whole can not return its initial fcc structure, resulting a large percentage in the amorphous state.

Here we will analyze in details only the case at lower velocity, 1.5 km/s. From the snapshots showed in Figure 11, we can see that at 1.2 ps the projectile hits the target producing an increase in temperature at the impact zone. Then the projectile continues to move through the target producing, in addition to local temperature increases (in the vicinity of the projectile trajectory), a wake of disturbed material, which is perceived as temperature fluctuations. At 4.8 ps dislocations appeared. When the projectile begins to leave the target, at 8.4 ps, some target atoms are ejected. At this same time, the area where the bullet impacts begins to become disordered. After a longer time, at 15 ps, the area where the projectile leaves the target (back side) is disordered. Finally, at 28.2 ps, we observe that the whole area which had been disturbed by the projectile is re-ordered, resembling its original structure, but with dislocations. In general, it appears that the projectile disturbs the zone which corresponds to its trajectory and its neighborhood, but it does not causes great impact beyond that (Loyola, 2010).

In order to quantify the just described picture, we analyze the change of local temperature, and the atomic order, by means of $g(r)$ and by the CNA. Temperature profiles are shown in Figs. 12, 13, which correspond to a radial zone close and far to bullet trajectory, respectively. In

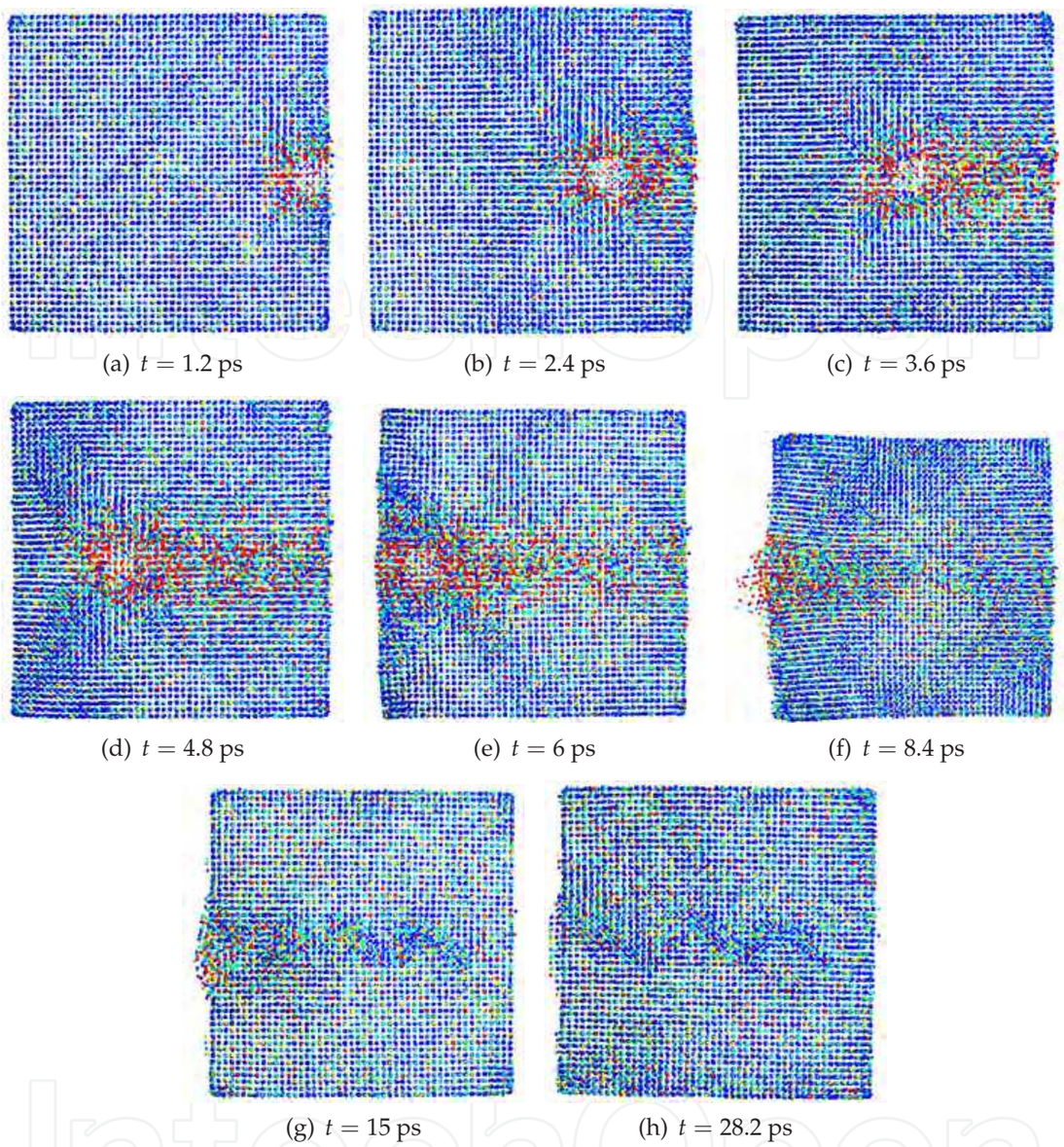

(a) $t = 1.2$ ps (b) $t = 2.4$ ps (c) $t = 3.6$ ps

(d) $t = 4.8$ ps (e) $t = 6$ ps (f) $t = 8.4$ ps

(g) $t = 15$ ps (h) $t = 28.2$ ps

Fig. 11. Snapshots of the impact of the projectile traveling at 1.5 km/s over a copper target at different times. The colors are assigned according to the atom's temperature, from low temperature (blue) to high temperature (red) (Loyola, 2010).

general, we can observe a temperature front that is moving in the same direction as the bullet. In Fig. 12 can be seen a temperature maxima of 1760 K at 3.6 ps. After that, at 28.2 ps, this part of the sample is thermalized at 450 K. The temperature, of course, propagates in radial direction from the center outward of the sample. Figure 13 displays the temperature profile beyond the central zone. Although there are not prominent peaks, the information about the passage of the projectile is shown in the 1.2 ps panel as a small peak at 65 Å , indicating that the temperature perturbation propagates at higher velocity than the projectile, ruling out the occurrence of a shock wave.

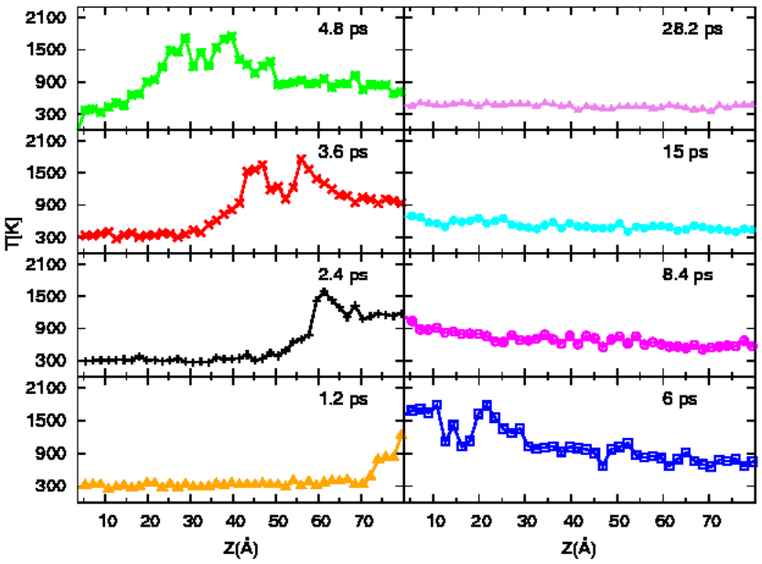


Fig. 12. Local temperature along the $z-$direction for different times, in the zone close to the center of the target, as the 1.5 km/s projectile is moving.

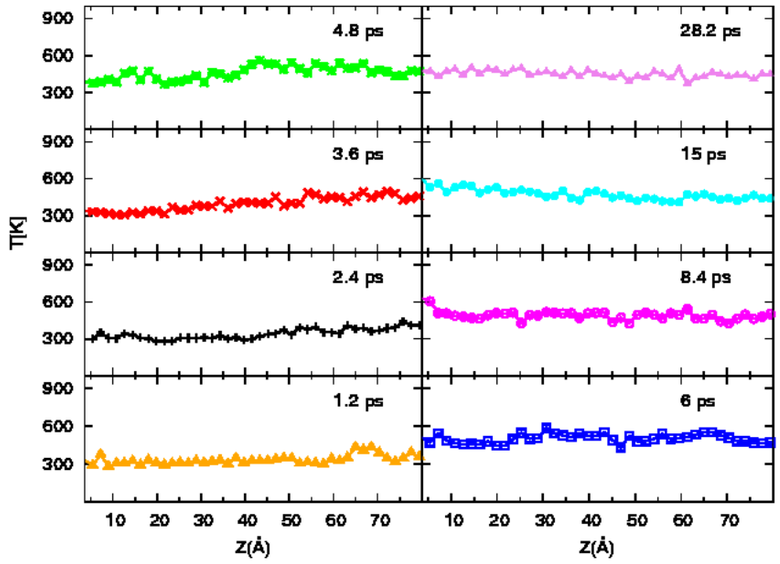


Fig. 13. Local temperature along the $z-$direction for different times, in the zone far the center of the target, as the 1.5 km/s projectile is moving.

The structural analysis of the sample was made by the pair distribution function, $g(r)$ for three different region in the $z$ direction: region A, where the bullet hit the sample (Fig. 14 a), region B, in the middle (Fig. 14 b), and region C, at the end of the sample (Fig. 14 c), where the bullet

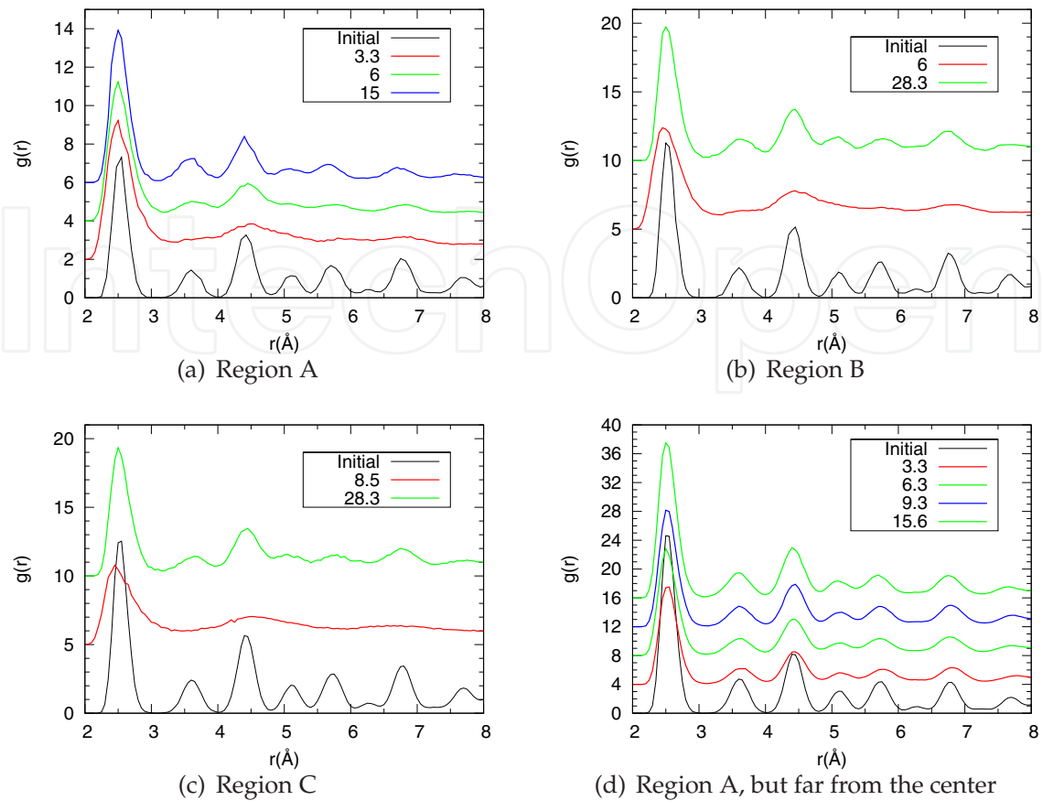


(a) Region A (b) Region B

(c) Region C (d) Region A, but far from the center

Fig. 14. Pair distribution function for different region of the sample. The curves have been shifted for clarity

go out. Figures 14 a, and 14 b show the same phenomenology but at different times. Initially, all sections have fcc structure (the peaks have a finite width because initially the system is at room temperature), then melt, as is appreciated at the times 3.3 ps, 6 ps and 8.5 ps for regions A, B and C, respectively. Finally, all these regions recover their crystalline structure, but at higher temperatures than the initial stage. In the case of the radial zone far from the bullet trajectory the situation is different because this part did not melt at any time, preserving the initial fcc structure but at higher temperatures, around 500 K.

Interestingly, the crystalline structure that the sample recovers after the passage of the bullet is a mixture between fcc and hcp structure. In fact, the high pressure resulting by the impact produce structural transformation, which at the end results in the coexistence of fcc and hcp phases. To quantify its relation, we perform a common neighbors analysis, CNA, for the the three region where the projectile pass, at the beginning (region A), the middle (region B) and the end (region C), with respect to the $z$ direction. The CNA calculates the percentage of atoms with structure fcc, hcp, bcc and icosahedral, and the rest is considered as non-crystalline (amorphous) structure. Figure 15 displays the percentage of fcc and hcp atoms (the difference between their sum and 100% corresponds to atoms in amorphous structure). We can see that in the region A, for $t < 2$ ps, all the atoms are still in a fcc order, because the bullet is just hitting. After that, the percentage of fcc atoms decrease to 10% and the hcp atoms appear, reaching also almost 10%. The rest are atoms in a non-crystalline structure. At $t > 8.5$ ps, when the projectile has go out the sample, the region A start to recover its crystalline order,

most atoms in fcc order. Finally, at $t = 28$ ps, the region reach 70% of fcc atoms, 3% of hcp atoms and around 25% of non-crystalline atoms. For the others regions the situation is similar, except it occurs at longer times, when the perturbation and the bullet reach that regions. The only significant difference is that, in the case of region C, the percentage of atoms in a non-crystalline structure is greater than the previous regions, which can be also seen directly from the snapshot (Fig. 11(h)).

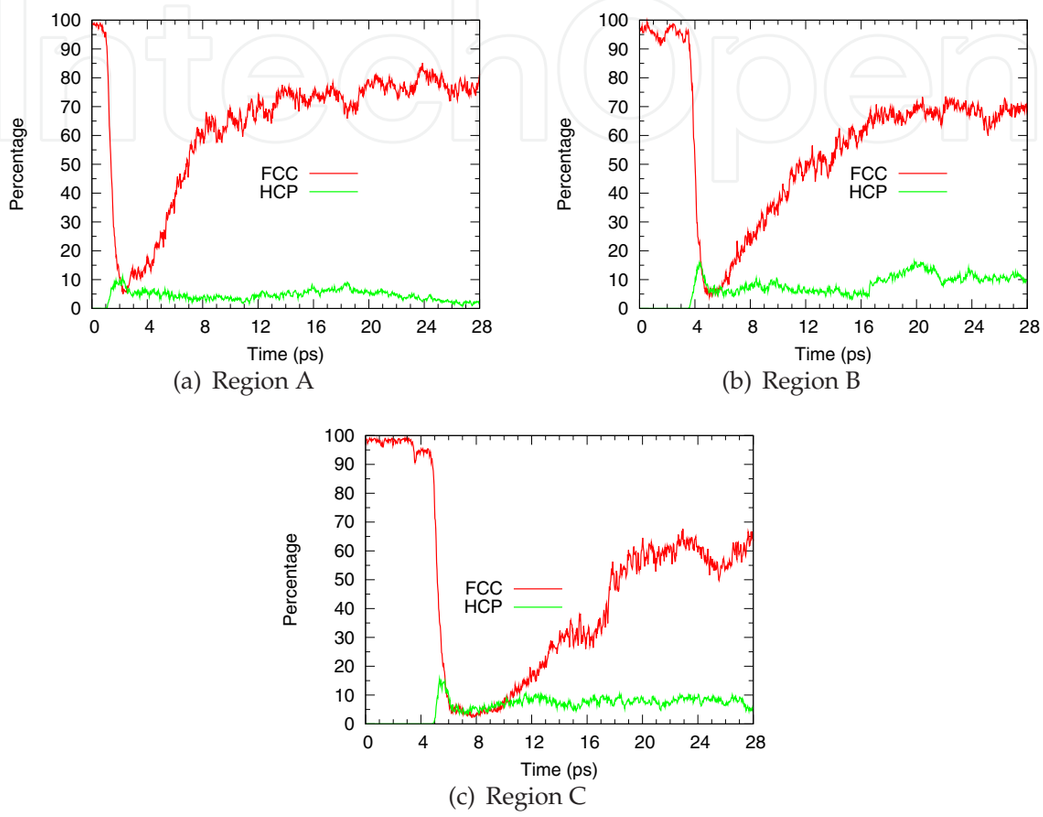


(a) Region A (b) Region B

(c) Region C

Fig. 15. Common neighbors analysis (CNA) at different times, for three region in the $z$ direction.

In summary, molecular dynamics simulation of hypervelocity projectile impact has been done. The atomic level study allows us to describe several interesting features that are not possible to track by other methods. In particular, two regimes has been identified, in dependence of the projectile initial velocity. At high velocity, the passage of the projectile through the target leaves a hole in the sample, as well as produce structural phase transition. Al low temperature, the case that has been study in detail here, the projectile cause local melting and dislocations as it moves through the sample. At the end, the target recover its original fcc crystalline structure, but with a non-negligible percentage of atoms in hcp structure and amorphous phase.

## 6. Conclusions

Descriptions of phenomena far from equilibrium are not an easy task in physics: from the experimental point of view it is required to have both high spatial and temporal resolution in the different variables measured; even worse, often we have destructive experiments, such as

projectile impact. From a theoretical standpoint, it is known that there is not a formalism that allows generally treatment of these systems, except in the case of linear response. This is where computer simulation provides valuable services, allowing for an atomic description of the phenomenon, taking into account the entire trajectory of the system. This was precisely what we do here, using a comprehensive computer code developed by us, for two cases of interest, namely inelastic impact and hypervelocity impact. In the first case, we were able to separate the various contributions of energy and revealed how they are transferred between them. Our results show that the most important transferable energy is the one between the ball-surface atoms, which grows during the impact and is zero at the others cases. Thus, this energy allows us to define a time of impact, which is approximately 1/10 the time between bounces. For the case of hypervelocity impact, we showed that molecular dynamics simulation reveals that exist a thresholds of materials behavior respect to projectile velocity: beyond certain velocity, in our case 4 km/s, the sample left with a permanent structural damage, expressed as a permanent hole in the center of the sample.

## 7. Acknowledgments

This work was supported by the Anillo Project ACT-24 *Computer simulation lab for nano-bio systems.* G. Gutiérrez thanks ENL 10/06 VRID-Universidad de Chile. F. González-Cataldo thanks CONICYT-Chile Ph.D fellowship. S. Davis acknowledges Fondecyt grant 3110017.

## 8. References

Aguirregabiria, J., Hernández, A. & Rivas, M. (2008). A simple model for inelastic collisions, *American Journal of Physics* 76(11): 1071.

Alonso, M. & Finn, E. (1992). *Physics*, Addison Wesley.

Baranyai, A. (2000). Temperature of nonequilibrium steady-state systems, *Phys. Rev. E* 62: 5989–5997.

Barrat, J. & Bocquet, L. (1999). Large slip effect at a nonwetting fluid-solid interface, *Physical Review Letters* 82(23): 4671–4674.

Bridges, F., Hatzes, A. & Lin, D. (1984). Structure, stability and evolution of saturn's rings, *Nature* 309: 333–335.

Callen, H. (1985). *Thermodynamics and an Introduction to Thermostatistics*, Wiley.

Casas-Vásquez, J. & Jou, D. (2003). Temperature in non-equilibrium states: a review of open problems and current proposals, *Rep. Prog. Phys.* 66: 1937–2023.

Davis, S., Loyola, C., González, F. & Peralta, J. (2010). Las palmeras molecular dynamics: A flexible and modular molecular dynamics code, *Computer Physics Communications* 181(12): 2126 – 2139.
URL: *http://www.sciencedirect.com/science/article/pii/S001046551000336X*

Dewar, R. (2005). Maximum entropy production and the fluctuation theorem, *J. Phys. A* 38(21): L371.

Dewar, R. C. (2003). Information theory explanation of the fluctuation theorem, maximum entropy production and self-organized criticality in non-equilibrium stationary states, *J. Phys. A: Math. Gen.* 36: 631.

Eisberg, R. & Lerner, L. (1981). *Physics: Foundations and Applications*, McGraw-Hill Inc.

Evans, D. & Searles, D. (2002). The fluctuation theorem, *Advances in Physics* 51(7): 1529–1585.
URL: *http://www.tandfonline.com/doi/abs/10.1080/00018730210155133*

Falcon, E., Laroche, C., Fauve, S. & Coste, C. (1998). Behavior of one inelastic ball bouncing repeatedly off the ground, *Eur. Phys. J. B* 3: 45–57.

Goldsmith, W. (2001). *Impact*, Dover Publications.

Gutiérrez, G., Menéndez-Proupin, E., Loyola, C., Peralta, J. & Davis., S. (2010). Computer simulation study of amorphous compounds: structural and vibrational properties, *Journal of Material Science* 45: 5124–5134. DOI: 10.1007/s10853–010–4579–0.

Hatzes, A. P., Bridges, F. G. & Lin, D. N. C. (1988). Collisional properties of ice spheres at low impact velocities, *Mon. Not. R. Astr. Soc.* 231: 1091.

Holian, B. L. (1995). Atomistic computer simulations of shock waves, *Shock waves* 5: 149–157.

Honeycutt, J. & Andersen, H. (1987). Molecular dynamics study of melting and freezing of small lennard-jones clusters, *Journal of Physical Chemistry* 91(19): 4950–4963.

Hoover, W. & Hoover, C. G. (2007). Computational physics with particles, *Am. J. Phys.* 76: 481.

Hsieh, H., Averback, R. S., Sellers, H. & Flynn, C. P. (1992). Molecular-dynamics simulations of collisions between energetic clusters of atoms and metal substrates, *Physical Review B* 45: 4417.

Jacquet, D. & Beyec, Y. L. (2002). Cluster impacts on solids, *Nuclear Instruments and Methods in Physics Research B* 193: 227.

Jaynes, E. T. (1980). The minimum entropy production principle, *Annu. Rev. Phys. Chem.* 31: 579.

Johnson, K. (1987). *Contact Mechanics*, Cambridge University Press.

Kirkpatrick, A. (2003). Gas cluster ion beam applications and equipment, *Nuclear Instruments and Methods in Physics Research B* 206: 830.

Kittel, C. (2005). *Introduction to Solid State Physics*, eighth edn, John Wiley & Sons, Inc, University of California, Berkeley.

Kleidon, A., Lorenz, R. & Lorenz, R. D. (2005). *Non-equilibrium thermodynamics and the production of entropy: life, earth, and beyond*, Springer.

Lifshitz, J. & Kolsky, H. (1964). Some experiments on anelastic rebound, *Journal of the Mechanics and Physics of Solids* 12(1): 35–43.
URL: *http://www.sciencedirect.com/science/article/pii/0022509664900055*

Loyola, C. (2010). *Material Behavior at Atomic Level: A Computer Simulation Study*, PhD thesis, Departamento de Física, Facultad de Ciencias, Universidad de Chile, Chile.

Loyola, C., Davis, S., Peralta, J. & Gutiérrez, G. (2010). Onset of failure in solid argon by the effect of a shockwave: a molecular dynamics study, *Computational Materials Science* 49: 582–587. DOI 10.1016/j.commatsci.2010.05.052.

Lun, C. & Savage, S. (1986). The effects of an impact velocity dependent coefficient of restitution on stresses developed by sheared granular materials, *Acta Mechanica* 63: 15–44. 10.1007/BF01182538.
URL: *http://dx.doi.org/10.1007/BF01182538*

Popok, V. N. & Campbell, E. E. B. (2006). Beams of atomic clusters: Effect on impact with solids, *Reviews on Advanced Materials Science* 11: 19.

Prigogine, I. (1968). *Introduction to thermodynamics of irreversible processes*, Interscience Publishers.

Raman., C. V. (1918). The photographic study of impact at minimal velocities, *Phys. Rev.* 12: 442–447.
URL: *http://link.aps.org/doi/10.1103/PhysRev.12.442*

Reed, J. (1985). Energy losses due to elastic wave propagation during an elastic impact, *Journal of Physics D: Applied Physics* 18: 2329.

Refson, K. (2000). Moldy: a portable molecular dynamics simulation program for serial and parallel computers, *Computer Physics Communications* 126(3): 310 – 329.
URL: *http://www.sciencedirect.com/science/article/pii/S0010465599004968*

Smith, W. & Forester, T. (1996). Dl_poly_2.0: A general-purpose parallel molecular dynamics simulation package, *Journal of Molecular Graphics* 14(3): 136 – 141.
URL: *http://www.sciencedirect.com/science/article/pii/S0263785596000434*

Stock, G., Ghosh, K. & Dill, K. A. (2008). Maximum caliber: A variational approach applied to two-state dynamics, *J. Chem. Phys.* 128: 194102.

Supulver, K., Bridges, F. & Lin, D. (1995). The coefficient of restitution of ice particles in glancing collisions: Experimental results for unfrosted surfaces, *Icarus* 113: 188–199.

Tabor, D. (1948). A simple theory of static and dynamic hardness, *Proceedings of the Royal Society of London. Series A. Mathematical and Physical Sciences* 192(1029): 247–274.
URL: *http://rspa.royalsocietypublishing.org/content/192/1029/247.abstract*

Tillett, J. (1954). A study of the impact of spheres on plates, *Proceedings of the Physical Society. Section B* 67: 677.

Tsai, Y. & Kolsky, H. (1967). A study of the fractures produced in glass blocks by impact, *Journal of the Mechanics and Physics of Solids* 15(4): 263–278.
URL: *http://www.sciencedirect.com/science/article/pii/0022509667900166*

Zener, C. (1941). The intrinsic inelasticity of large plates, *Phys. Rev.* 59: 669–673.
URL: *http://link.aps.org/doi/10.1103/PhysRev.59.669*

Zukas, J., Nicholas, T., Swift, H., Greszczuk, L. & Curran, D. (1982). *Impact Dynamics*, John Wiley & Sons Inc.

Zwanzig, R. (2001). *Nonequilibrium Statistical Mechanics*, Oxford University Press.

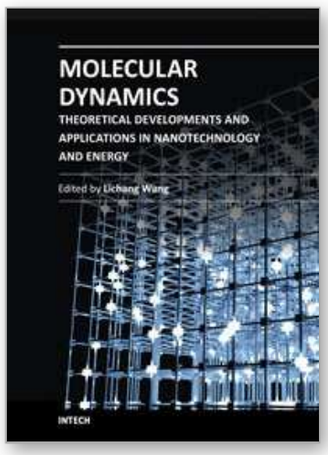


**Molecular Dynamics - Theoretical Developments and Applications in Nanotechnology and Energy**

Edited by Prof. Lichang Wang

ISBN 978-953-51-0443-8
Hard cover, 424 pages
**Publisher** InTech
**Published online** 05, April, 2012
**Published in print edition** April, 2012

Molecular Dynamics is a two-volume compendium of the ever-growing applications of molecular dynamics simulations to solve a wider range of scientific and engineering challenges. The contents illustrate the rapid progress on molecular dynamics simulations in many fields of science and technology, such as nanotechnology, energy research, and biology, due to the advances of new dynamics theories and the extraordinary power of today's computers. This first book begins with a general description of underlying theories of molecular dynamics simulations and provides extensive coverage of molecular dynamics simulations in nanotechnology and energy. Coverage of this book includes: Recent advances of molecular dynamics theory Formation and evolution of nanoparticles of up to 106 atoms Diffusion and dissociation of gas and liquid molecules on silicon, metal, or metal organic frameworks Conductivity of ionic species in solid oxides Ion solvation in liquid mixtures Nuclear structures



**InTech Europe**
University Campus STeP Ri
Slavka Krautzeka 83/A
51000 Rijeka, Croatia
Phone: +385 (51) 770 447
Fax: +385 (51) 686 166
www.intechopen.com

**InTech China**
Unit 405, Office Block, Hotel Equatorial Shanghai
No.65, Yan An Road (West), Shanghai, 200040, China
中国上海市延安西路65号上海国际贵都大饭店办公楼405单元
Phone: +86-21-62489820
Fax: +86-21-62489821

IntechOpen